VIII International Conference on Computational Methods in Marine Engineering
MARINE 2019
R. Bensow and J. Ringsberg (Eds)

PREDICTION OF SHIP RESISTANCE WITH THE USE OF FULL-SCALE CFD SIMULATIONS

MARINE 2019

KAROL NIKLAS*, HANNA PRUSZKO*

* Faculty of Ocean Engineering and Ship Technology
Gdansk University of Technology
Narutowicza 11/12, 80233 Gdansk, Poland
e-mail: karol.niklas@pg.edu.pl, www.oio.pg.edu.pl/about

Key words: Computational Methods, Marine Engineering, CFD, Ship Resistance

Abstract. In recent years, the IMO has introduced new regulations to reduce the negative impact of ships on the natural environment. A particularly important step forcing technological innovations is the increasing requirement of ship energy efficiency. It is expressed by the Energy Efficiency Design Index (EEDI). Another important step towards green shipping is raising the required quality of fuel used for propulsion, the so-called Tier limits. Higher demand of Low Sulfur Fuel Oil resulted in its price rising up by 200% in the past two years. All these aspects increase the importance of ship fuel economy. As a result, the hull resistance reduction plays a significant role in the design process of new vessels. For vessels operating at sites with moderate and rough waves, the shape of the hull and, in particular, the bow section plays an important role. The paper presents results of some of the research carried out as a part of the "Smart Propulsion System" research project. The presented stage of the work includes a full-scale CFD simulation for a case study ship redesigned from an as-built V-shaped bulbous bow to three different innovative variants. Changes in the hull form were made in such a way that the redesigned hull versions preserved the main dimensions and hydrostatic parameters of the original design. The paper presents ship resistance analysis on calm water as a part of seakeeping analysis. The scope of the work was full-scale CFD simulations of four innovative hull forms in order to determine total resistance, dynamic trim and sinkage. The influence of bow and stern shape, wetted surface area and waterplane area on total resistance was investigated. Main conclusions were formulated for the novel hull forms being analysed. The scope of further work was formulated, and it included assessment of the combined influence of the ship's speed and waving conditions on the performance at a specific operational site. To reduce fuel consumption, the optimal design and operation of the ship are equally important and can be supported by full-scale CFD simulations.

1 INTRODUCTION

Accurate and reliable determination of ship resistance by CFD simulations is of great importance. The methodology is described by the ITTC recommended practice [1], [2] and quite often used by different researchers for hydrodynamic analyses. The wave pattern, wake and resistance of a fully appended ship were studied numerically in [3]. In paper [4], numerical simulations as a powerful tool to compute viscous flows and a way to improve prediction of

full-scale resistance were presented. In [5], simulations of calm water resistance and seakeeping performance were presented. Numerous papers address the potential of hull form optimization using numerical methods. In [6], slender body approximation was used to compute wave resistance and find optimum shape among series of eight hull forms. Parametric modelling of hull shape was also presented in [7]. The possible application of RANSE was discussed, as well as robustness and efficiency of numerical simulations. Different optimization techniques can be applied. The one studied in [8] was an evolutionary technique used for hull resistance optimization taking as a starting point the Wigley hull form. The Boundary Element Method was used in [9] for optimisation of the parametric model of hull forms that were created based on T-splines. Shape of the bow was also of great interest. For example, [10] created the generation of bulbous bows with a goal of drag reduction. New forms were analysed numerically and experimentally. CFD simulations were also used as a tool to investigate more sophisticated methods of ship resistance analysis. The effect of coating and biofouling was studied in [11]. Drag reduction of superhydrophobic surfaces was investigated in [12]. In the articles [13], [14], [15], the CFD simulation of a full-scale ship with self-propulsion was presented. Simulations of ship maneuverability were presented in [16]. The method was applied also in unusual offshore applications, i.e. [17], [18], [19].

2 AIM AND SCOPE

The aim of the study was to investigate the influence of the hull form of the case study vessel on calm water performance. The selected hull forms represent the most recognised examples of concepts recently developed by different design offices.

The scope of the work included full-scale simulations of four variants of hull shape. The compared concepts were similar to: V-shaped bulbous bow, X-bow, X-bow-X-aft, and B-bow. The X-bow [20] and X-aft concepts were developed by the Ulstein company. The concept denoted as B-bow was developed by the Havyard company. The total resistance and its components (frictional and pressure resistance), dynamic trim and sinkage were analysed. The paper presents a part of the research on the application of full-scale CFD simulations into ship design and operation for increasing energy efficiency, comfort and safety of ships.

In Section 3, the case study vessels were described. In Section 4, the setup of numerical simulations was presented. In Section 5, results were analysed. In Section 6, conclusions and recommendations for further study were described.

3 THE CASE STUDY VESSEL AND HULL FORM VARIANTS

For the purpose of research, the case study vessel Nawigator XXI (IMO: 9161247) was selected. She is a training and research vessel operating mainly on the Baltic Sea. The hull form characteristics are transom stern, full midship section and V-shaped bulbous bow with a flare. The ship in the as-built version was denoted as CSV1. The hull form was redesigned according to selected innovative variants in such a way to preserve the main dimensions and hydrostatic parameters. The body forms were denoted from CSV2 to CSV4. The main particulars are presented in Table 1. The side views of CSV1–CSV4 are presented in Fig. 1.

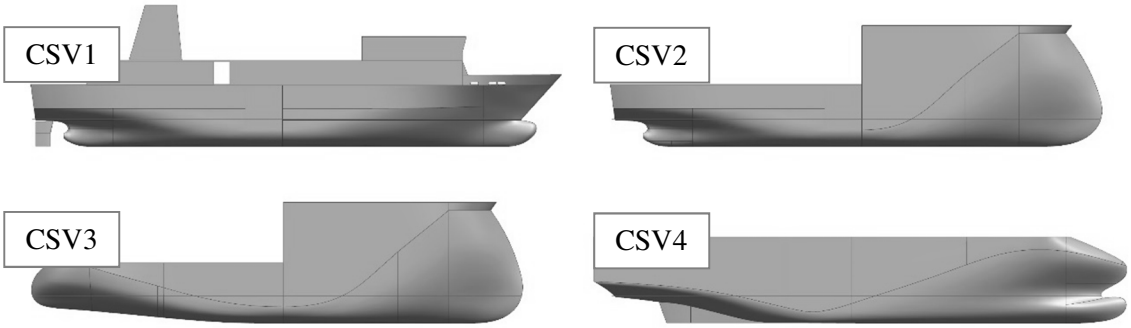

Figure 1: Hull forms of the case study vessel: CSV1 – V-shaped bulbous bow and transom stern; CSV2 – X-bow and transom stern; CSV3 – X-bow and X-aft (cruiser stern); CSV4 – B-bow and V-shaped transom stern

Table 1: Main particulars of CSV1–CSV4 hull forms

Name	unit	CSV1	CSV2	CSV3	CSV4
Waterline length L_{WL}	(m)	55.68	55.15	55.50	55.24
Breadth B	(m)	10.50	10.50	10.50	10.50
Drought T	(m)	3.14	3.14	3.14	3.14
Displacement D	(m^3)	1110	1109	1110	1110
Wetted surface area S_W	(m^2)	677.3	652.6	648.4	690.9
Waterplane area S_{WP}	(m^2)	473.3	456.4	468.3	447.6
Longitudinal centre of buoyancy L_{CB}	(%L_{WL})	46.70	47.94	48.69	51.90
Vertical position of centre of gravity Z_G	(m)	4.16	4.16	4.16	4.16
Gyradius k_{YY}	[-]	0.219	0.219	0.219	0.219

4 FULL-SCALE CFD SIMULATION FOR THE DETERMINATION OF CALM WATER RESISTANCE

Numerical methods allow us to solve the discretised governing equations of mass, momentum and energy conservation that are commonly known as the Navier–Stokes equations. Depending on the problem complexity, different simplifications might be applied. For naval applications, where fluid is assumed to be incompressible, only mass and momentum continuity are considered. However, the great complexity of the flow around a ship's hull does not allow for solving equations analytically, and numerical methods need to be applied.

To run CFD calculations, the commercial code STAR CCM+ was used. The solver uses a finite volume method that discretises the whole computational domain and iteratively solves the integral version of the transport equations. The flow was solved as three-dimensional, turbulent, viscous, incompressible and multiphase. In order to capture the interface between phases, a surface-capturing VOF (Volume of Fluid) model was applied. The turbulent flow was modelled using the RANS approach. This method is based on the assumption that instantaneous velocity can be represented by the sum of mean and fluctuating components. Those values are then averaged and inserted into the N-S equations. The averaging process involves introducing additional terms that increase the number of unknown values in the RANS equations. To solve the closure problem, the turbulence model needs to be applied [21]. The k–ε model with all y+

treatment was applied for simulations. This model offers a good compromise between robustness and accuracy. The model is also a frequent choice when using STAR CCM+ software [22], [23]. For spatial discretisation, a second-order upwind numerical scheme was used for the convection term, and a first-order implicit scheme was used for temporal discretisation. The time step of the numerical simulations varied according to the vessel's speed in order to satisfy the Courant–Friedrichs–Lewy condition, defined by Equation 1. In the formula, Δt stands for a time step, Δx is a grid size in the direction of a flow velocity vector, u is velocity, and C is a constant. For naval applications, it is recommended that C is equal to 0.5–0.7 for a free surface and 5–10 for a hull surface [21].

$$\frac{u \cdot \Delta t}{\Delta x} \leq C \qquad (1)$$

To compute the motions of a ship as a response to fluid forces, the DFBI model (Dynamic Fluid Body Interaction) was applied. This module allows to integrate the pressure and shear forces over the surface of a body. Acting forces and moments are used to find, in an iterative way, the new position of an object after translational motion and angular rotation of a body's centre of mass [24]. Four degrees of freedom were restrained, and the model was allowed to sink and trim.

The size of the domain and ship position were specified in order to capture the Kelvin wave pattern and also to avoid reflection from the side and downstream boundary. For the same reason, numerical wave damping was applied on these boundaries. The computational domain is presented in Figure 2. The setup of the numerical domain is presented in Table 2.

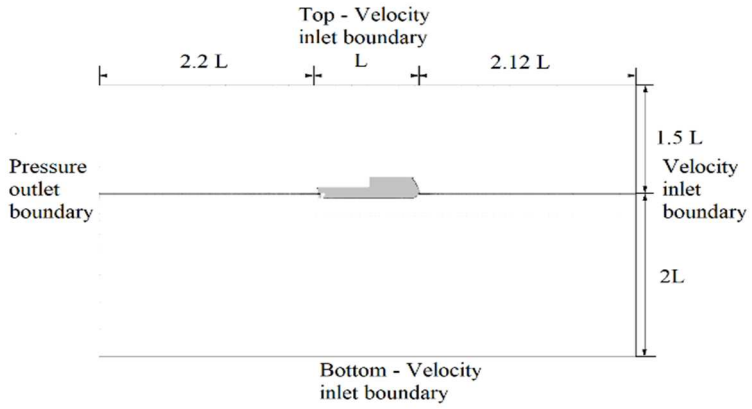

Figure 2: Computational domain and boundary conditions

Table 2: Boundary conditions

Boundary	**Position**	**Boundary Condition**
Inlet	2.12 L_{pp} in front of a ship	Velocity inlet
Outlet	2.2 L_{pp} behind a ship	Pressure outlet
Symmetry	Symmetry plane of a ship	Symmetry
Side	2.2 L_{pp} from symmetry plane	Velocity inlet
Top	1.5 L_{pp} above free surface	Velocity inlet
Bottom	2 L_{pp} below free surface	Velocity inlet

The discretisation of the volume was performed according to a recent state-of-art method. Grid refinements were applied in a way to make it possible to capture the most important features of the flow. This included increasing the mesh resolution in the free surface, wake and closest proximity to the hull surface where prism layers were used in the region of the boundary layer — see Figure 3. The mesh resolution in the region of the ship's boundary layer resulted in a value of y+ within a range of 30–50. The approach with a symmetry plane of a ship was used, and the total number of volumetric cells was equal to 2.1 million for the CSV1. To allow for objective comparison between hulls, all four meshes were designed in the same way, resulting in the same grid resolution in the region of the boundary layer and refinements in the region around the hulls. However, due to features of the hull shape such as bulbous bow or propeller shaft tube the total number of cells was slightly different for each mesh. The total number of cells for each variant is presented in Table 3.

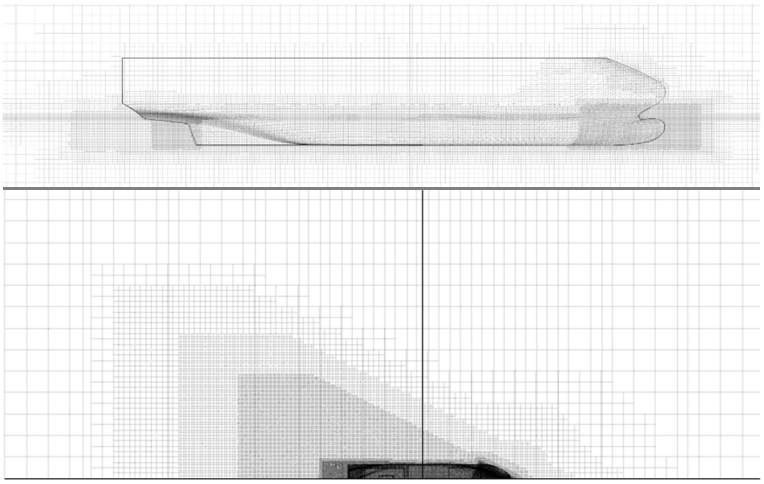

Figure 3: Computational mesh – side and top view

Table 3: Number of cells for hull variants CSV1–CSV4

	CSV1	CSV2	CSV3	CSV4
No. of cells	2.1 M	2.1 M	2.2M	2.2 M

Computations were performed for a range of speed from 5 to 13 knots with 1 knot increment in range from 7 to 13 knots. This corresponds to a Froude number F_N from 0.11 to 0.29.

In order to assess the accuracy of the numerical solution, a verification study was performed. The verification study was carried out for CSV1 for two coarser meshes with total cell number equal to 1 M and 0.5 M cells for vessel speed of 10 knots. This follows the ITTC procedure for verification and validation of CFD computations [25]. The results are presented in Table 4. The simulations were characterised by monotonic convergence with grid size error equal to 0.8% and corrected grid size uncertainty equal to 0.22%.

Table 4: Results of the verification study

Ship velocity [knots]	F_N [-]	Grid refinement ratio R_G [-]	Correction factor C_G [-]	Grid size uncertainty U_G [%S]	Grid size error δ_G^* [%S]	Corrected grid uncertainty U_{G_C} [%S]
10	0.22	0.44	0.74	0.86%	0.80%	0.22

4 RESULTS

The results of total resistance for all analysed hull form variants are presented in Table 5. The calculated speed range was from 5 to 13 knots (F_N from 0.11 to 0.29). For each speed, the lowest values of resistance are marked in **bold**, whereas the highest values of resistance are marked in *italics*.

Table 5: Results of total resistance R_T for hull variants CSV1–CSV4

Speed [knots]	F_N [-]	CSV1 R_T [kN]	CSV2 R_T [kN]	CSV3 R_T [kN]	CSV4 R_T [kN]
5	0.11	***7.47***	6.59	**5.47**	6.29
7	0.15	***14.84***	13.10	**10.81**	11.67
8	0.18	***20.04***	17.71	**14.52**	15.26
9	0.20	***25.4***	23.54	19.64	**19.50**
10	0.22	***33.52***	31.42	**26.33**	29.1
11	0.24	***43.63***	41.20	**35.88**	38.42
12	0.26	56.62	***61.99***	**51.18**	53.42
13	0.29	**81.98**	***106.55***	84.97	95.85

For the speed corresponding to Froude number of $F_N \leq 0.24$, the vessel in the as-built variant (CSV1) had the highest resistance. For higher speed, the CSV2 had the highest total resistance. In the range of Froude number from 0.11 to 0.26 (5–12 knots), excluding $F_N = 0.2$ (9 knots), the CSV3 had the lowest resistance. It was the variant with a cruiser stern instead of a transom stern. For $F_N = 0.2$, the CSV4 had the lowest resistance. For the highest analysed speed of $F_N = 0.29$ (13 knots), the CSV1 had the lowest value of resistance. The hull form of CSV4 had relatively low resistance for the entire range of speed.

The results of the calculated total resistance coefficient are presented in Figure 4. For $F_N \leq 0.26$ (12 knots), the relative differences for the analysed variants of hull form were significant. For higher speeds, the difference in resistance performance increased much more rapidly. The comparison between variants CSV1 and CSV2 assessed the influence of the X-bow type bow shape. The comparison between CSV2 and CSV3 assessed the influence of a cruiser-type stern shape (X-aft). The comparison between CSV1, CSV3 and CSV4 assessed the influence of the hull form concept on the resistance performance.

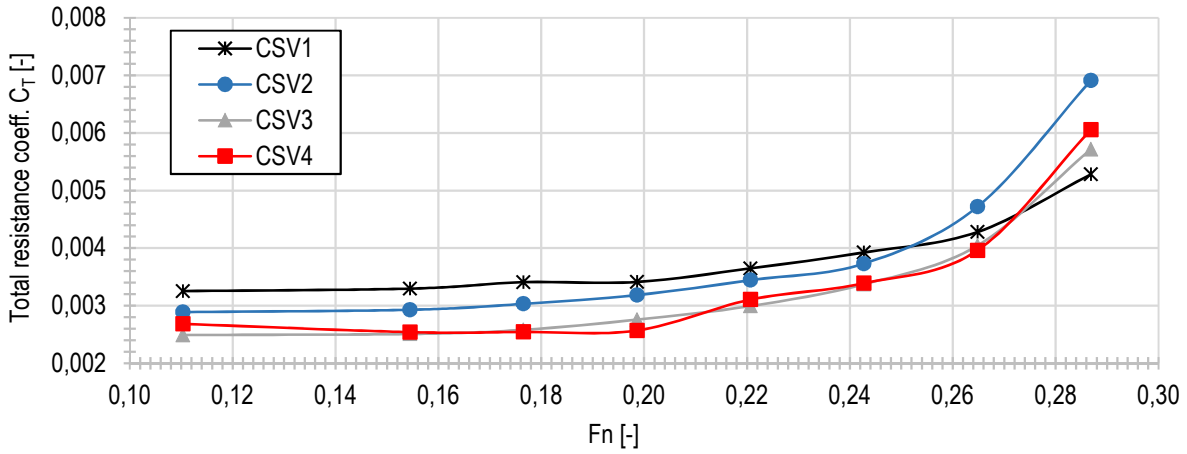

Figure 4: Total resistance coefficient for hull variants CSV1–CSV4

Vessels CSV1 and CSV2 had different bow forms. The replacement of the typical V-shaped bulbous bow by the X-bow form can be studied. For small Froude numbers, the CSV2 was characterised by lower resistance. For $F_N = 0.25$, the resistance curves intersected. For higher speed, the variant with bulbous bow was highly beneficial, and differences between total resistance coefficients increased with speed. This was a result of the reduction of pressure resistance by the bulbous bow. The comparison between variants CSV2 and CSV3 allowed to assess the influence of X-aft. It can be noticed that the resistance curves for CSV2 and CSV3 were almost parallel, and the variant with cruiser stern had lower resistance for the entire speed range. Transom sterns are applied on semi-planing and planing crafts and are beneficial for higher values of Froude number. The case study vessel operates in a displacement speed regime, thus the cruiser stern is supposed to be beneficial. The obtained results confirmed that expectation. Unlike the CSV3, for the CSV2 a hollow on the resistance curve for $F_N = 0.24$ (11 knots) and a hump for $F_N = 0.29$ (13 knots) occurred. Both hulls were subjected to significant increase of total resistance for speed above $F_N = 0.26$ (12 knots). The CSV4 has an atypically inclined stern that is supposed to damp transverse waves with a sharp waterline ending. This variant has an elongated and narrow bulbous bow with a conical flare. This bow form resembles the letter B. The CSV4 had reduced resistance in comparison to the CSV1 for $F_N < 0.27$. Despite the very different hull forms, the CSV3 and CSV4 had the most similar resistance for the entire speed range. The relative differences of resistance were equal 15%, 8%, 5%, –0.7%, 11%, 7%, 4%, 13% for F_N of 0.11, 0.15, 0.18, 0.20, 0.22, 0.24, 0.26, 0.28, accordingly. In Figure 5, the relative difference of the total resistance between the modified variants of the study vessel and the as-built (CSV1) version are shown. For F_N up to 0.24, the redesigned versions had significant reduction of hull resistance from –6% to –28%. For the design speed of $F_N = 0.22$ (10 knots), the reductions of total resistance for CSV2, CSV3, CSV4 were equal to –6%, –21%, –13%, accordingly. The resistance reduction for CSV2 varies between 6% and 12%, for CSV3 between 18% and 28%, and for CSV4 between 12% and 24%. For $F_N = 0.26$, the CSV2 had 9% higher resistance, and the remaining two vessels has 10% and 6% lower resistance. For $F_N = 0.29$, the CSV2–CSV4 had higher resistance than the CSV1 had, with up to 30% increase for CSV2.

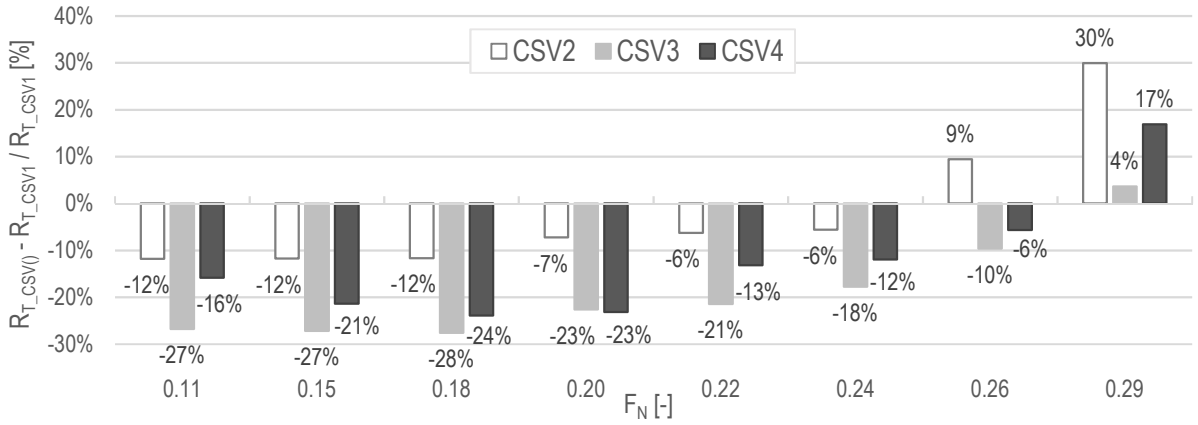

Figure 5: Relative change of total resistance caused by redesigning the hull CSV1 (as-built) to CSV2–CSV4

In Figure 6, pressure and frictional resistance coefficients are presented. The frictional resistance coefficient for all hull variants of the case study vessel were similar. This resulted from similar values of wetted surface area. For CSV1 and CSV4, the differences between values of frictional resistance for F_N = 0.15, 0.26 and 0.29 were less than 0.5%. For F_N between 0.25 and 0.26, pressure resistance became a bigger contributor to total resistance for all vessels, and its value started to increase rapidly. The humps and hollows of pressure resistance curves are visible. The CSV1 with a bulbous bow had much smaller pressure resistance for F_N above 0.27. For the entire range of speed, the CSV3 had the lowest frictional resistance due to the smallest wetted surface area.

Results of sinkage and dynamic trim are presented in Figure 7. It can be noticed that the smaller the area of waterplane, the higher the value of sinkage. The CSV1 was the only vessel that had negative value of dynamic trim, with bow up varying from –0.48 to –0.34 degrees. Other variants had dynamic trim with bow down. The highest value of running trim was equal to 0.6 degrees corresponding to F_N = 0.29 for CSV4. The CSV2 and the CSV3 had similar values of running trim, ranging between 0.1 and 0.31 degrees. For the CSV1–CSV2 hull forms and F_N = 0.26, the maximum value of running trim occurred.

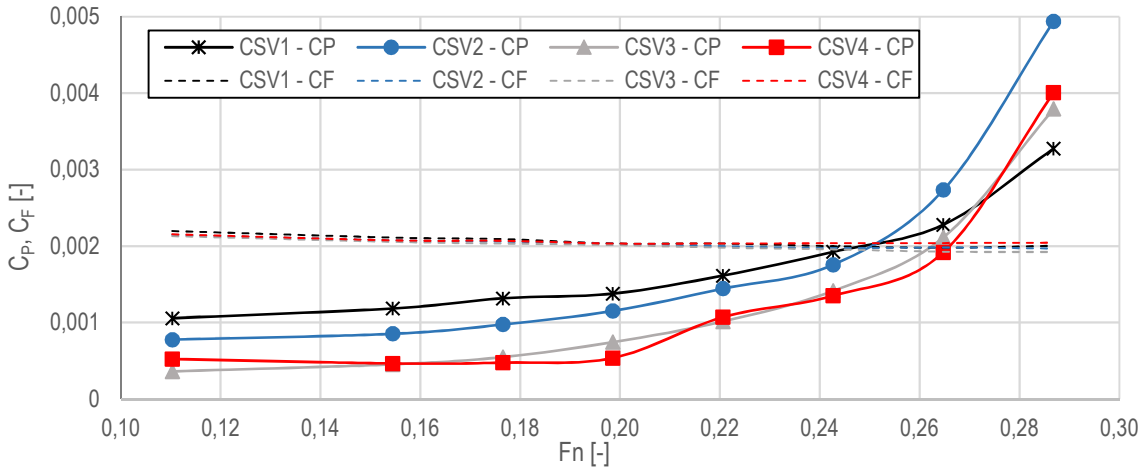

Figure 6: Pressure resistance coefficient C_P and frictional resistance coefficient C_F

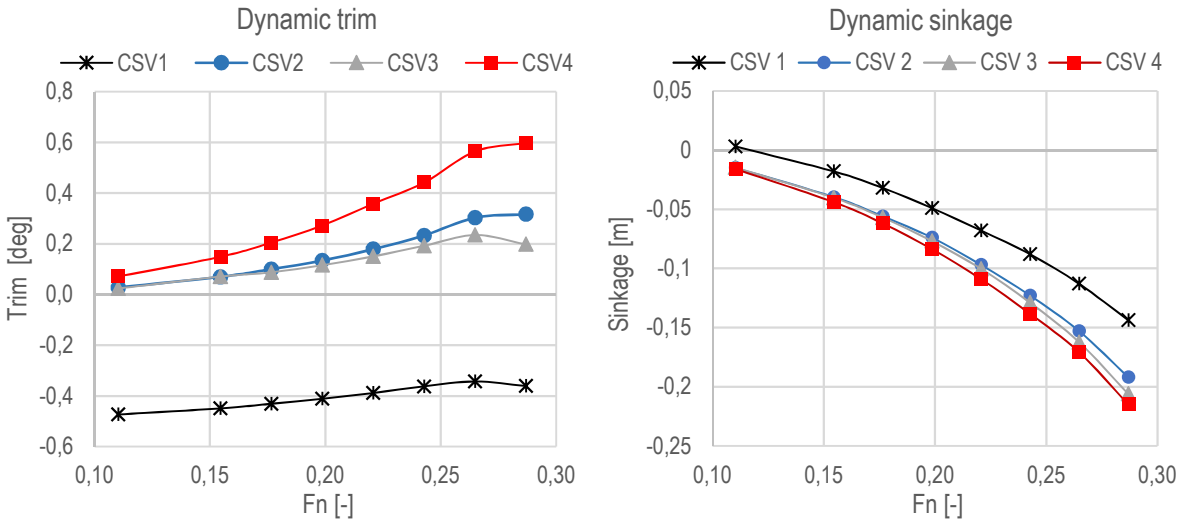

Figure 7: Dynamic trim and sinkage

In Figure 8, the relations between speed, wetted surface area S_W, waterplane area S_{WP}, and total resistance coefficient C_T are presented. On the left plot, hull variants are ranked from the one with the smallest wetted surface area, which in this case was the CSV3, to the one with the greatest — CSV4. The conclusion was that the wetted surface area for the analysed hull variants had minor impact on the value of total resistance. The difference of total resistance coefficient between CSV3 and CSV4 was slight. Furthermore, the CSV2 and CSV3, despite their moderate values of wetted surface area, had higher resistance than the CSV4 had. On the right plot, hull variants were ranked from CSV4 with the lowest waterplane area to CSV1 with the highest waterplane area. The conclusion was that the differences of waterplane area for the analysed hull variants had minor impact on the value of total resistance.

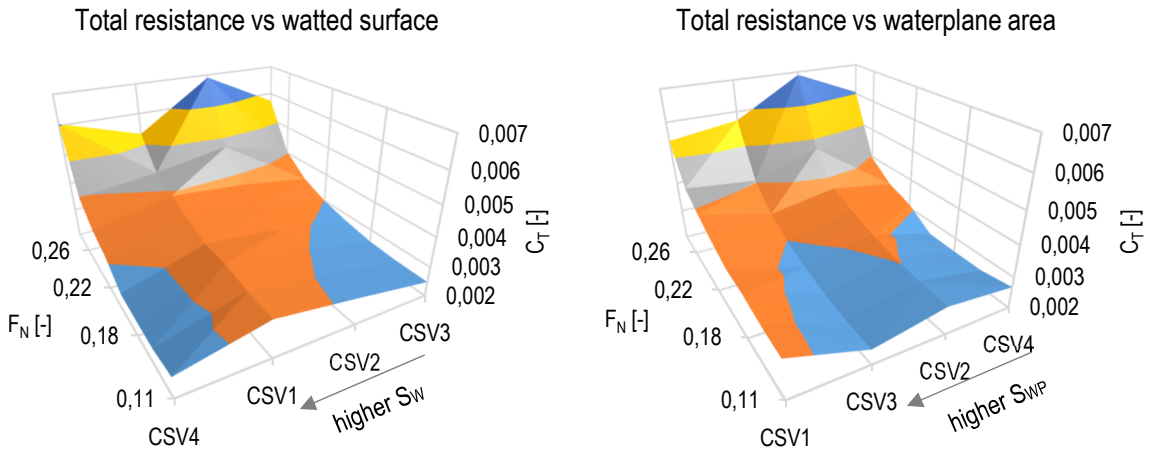

Figure 8: Influence of wetted surface area S_W and waterplane area S_{WP} on total resistance coefficient C_T

5 CONCLUSIONS

In upcoming years, due to new IMO regulations, the fuel economy of ships needs to be improved. Thus, the reduction of hull resistance will be increasingly important. The ship's design process can be significantly supported by full-scale CFD simulations giving a great possibility of proper hull form selection analysis. This paper demonstrated full-scale CFD simulations of calm water performance executed for four variants of a hull form. These four variants represent the innovative concepts of hull forms available on the commercial market. Namely, the V-shaped bulbous bow, X-bow, X-aft and B-bow. Analysis of the influence of hull form on calm water resistance was performed with the use of a case study vessel. The redesigned hull variants preserved the main hull dimensions and hydrostatic data, as well as the mass distribution. The following conclusions were formulated:

1. Full-scale CFD simulation can be used as a reliable and effective tool for resistance performance. The method takes advantage of directly modelling the ship's full scale. Thus, there is no need for extrapolation from a model scale to a full scale. This is important, especially for innovative and atypical hull forms with unknown form factor. Because of that, the determination of hull resistance with the use of towing tank testing has high uncertainty. The full-scale CFD simulations overcome this issue and can deliver the advantage of analysing many different hull forms evaluated both by an evolutionary and revolutionary approach.
2. The redesigned variants of the case study vessel, namely CSV2–CSV4, had significantly reduced resistance in a speed range from $F_N = 0.11$ (5 knots) to $F_N = 0.25$ (11.5 knots). For the operational speed corresponding to $F_N = 0.22$ (10 knots), the reduction of total resistance for CSV2, CSV3, CSV4 was equal 6%, 21%, 13%, accordingly. For lower speeds, the reduction was from 7% to 28%. For $F_N = 0.26$ (12 knots), the CSV3 and CSV4 had reduction of total resistance by 10% and 6%, accordingly. For the speed corresponding to $F_N = 0.29$ (13 knots), the CSV2–CSV4 had increased resistance in comparison with the original CSV1 hull form by 30%, 4%, and 17%, accordingly. This resulted from increased pressure forces acting on the hull starting to exceed frictional forces. As a consequence, a significant wave pattern developed around the hull. For the speed of $F_N = 0.29$ (13 knots), the original hull form benefited from the bulbous bow which greatly reduced the pressure component of resistance.
3. Reduction of resistance due to change of the stern shape from transom to X-aft (cruiser-type stern) was almost constant in a range of F_N from 0.11 to 0.24. The relative average difference between CSV2 and CSV3 was equal to 16%. For higher Froude numbers of $F_N = 0.26$ and $F_N = 0.29$, the reductions of resistance were equal to 17% and 20%, accordingly. The stern similar to the X-aft concept was better than the transom stern of the CSV1. For the displacement speed regime, a cruiser stern type should always be beneficial from the hydrodynamic point of view. Despite that, transom sterns are most frequently applied on merchant displacement ships. The reason for this can be much easier manufacturing. The transom stern is generally expected to provide better performance for speeds $F_N > 0.4$.

4. The redesigned hull variants CSV2–CSV4 had higher values of dynamic trim and sinkage than the original hull form CSV1 had. The CSV1 was the only vessel with initial trim bow up, varying from 0.34 degrees for F_N = 0.26 to 0.48 degrees for F_N = 0.11. The remaining hull variants had dynamic trim with bow down. The greatest trim angle was in the CSV4 for the maximum value of 0.6 degrees for F_N = 0.29. The CSV2 and CSV3 had very similar values of trim angle, varying from 0.1 to 0.32 degrees. For CSV3, the maximum trim angle wad equal to 0.24 degrees and occurred for F_N = 0.26, and CSV2 reached maximum trim angle equal to 0.32 degrees for F_N = 0.29. The highest sinkage equal was to 0.21 m and occurred for the maximum speed of CSV4. This vessel was characterised by the smallest waterplane area. The CSV1 had the lowest sinkage, and for the maximum speed it was equal 0.14 m.
5. Analysis of the waterplane area and wetted surface area influence allows to draw conclusions that both particulars had minor influence on the resistance of the analysed hull variants.
6. This article presented the crucial step of overall analysis as calm water resistance is necessary to assess the added resistance. A subsequent paper will investigate the influence of hull form on the seakeeping performance, especially on the added resistance and ship motions.

Acknowledgements
The research was supported by the National Centre for Research and Development (NCRD) and the SmartPS project No. MARTECII/SmartPS/4/2016. The research was supported by the Academic Computer Centre in Gdansk (CI TASK). All the support is highly appreciated by the authors.

REFERENCES

[1] ITTC, "ITTC – Recommended Procedures and Guidelines - Practical guidelines for ship CFD applications. 7.5-03-02-03 (Revision 01)," in *ITTC – Recommended Procedures and Guidelines*, 2014, p. 19.
[2] ITTC, "Practical Guidelines for Ship Resistance CFD - 7.5-03-02-04," in *ITTC – Recommended Procedures and Guidelines*, 2014, pp. 1–9.
[3] Z.-R. Zhang, H. Liu, S.-P. Zhu, and F. Zhao, "Application of CFD in ship engineering design practice and ship hydrodynamics," *J. Hydrodyn.*, vol. 18, iss. 3, suppl., pp. 315–322, 2006.
[4] H. C. Raven, A. van der Ploeg, A. R. Starke, and L. Eça, "Towards a CFD-based prediction of ship performance — Progress in predicting full-scale resistance and scale effects," *Trans. R. Inst. Nav. Archit. Part A Int. J. Marit. Eng.*, 2008.
[5] R. Broglia, B. Bouscasse, B. Jacob, A. Olivieri, S. Zaghi, and F. Stern, "Calm water and seakeeping investigation for a fast catamaran," *FAST 2011 11th Int. Conf. Fast Sea Transp.*, 2011.
[6] S. Percival, D. Hendrix, and F. Noblesse, "Hydrodynamic optimization of ship hull forms," *Appl. Ocean Res.*, 2001.
[7] J. J. Maisonneuve, S. Harries, J. Marzi, H. C. Raven, U. Viviani, and H. Piippo,

"Towards Optimal Design of Ship Hull Shapes," *8th Int. Mar. Des. Conf.*, 2003.
[8] H. Zakerdoost, H. Ghassemi, and M. Ghiasi, "An evolutionary optimization technique applied to resistance reduction of the ship hull form," *J. Nav. Archit. Mar. Eng.*, 2013.
[9] K. V. Kostas, A. I. Ginnis, C. G. Politis, and P. D. Kaklis, "Ship-hull shape optimization with a T-spline based BEM-isogeometric solver," *Comput. Methods Appl. Mech. Eng.*, 2015.
[10] F. Huang and C. Yang, "Hull form optimization of a cargo ship for reduced drag," *J. Hydrodyn.*, vol. 28, no. 2, pp. 173–183, 2016.
[11] Y. K. Demirel, O. Turan, and A. Incecik, "Predicting the effect of biofouling on ship resistance using CFD," *Appl. Ocean Res.*, 2017.
[12] Y. Li, K. Alame, and K. Mahesh, "Feature-resolved computational and analytical study of laminar drag reduction by superhydrophobic surfaces," *Phys. Rev. Fluids*, 2017.
[13] D. Ponkratov and C. Zegos, "Validation of ship scale CFD self-propulsion simulation by the direct comparison with sea trials results," in *4th Int. Symp. Marine Propulsors*, 2015.
[14] S. Bhushan, T. Xing, P. Carrica, and F. Stern, "Model- and full-scale URANS simulations of Athena resistance, powering, seakeeping, and 5415 maneuvering," *J. Sh. Res.*, vol. 53, no. 4, pp. 179–198, 2009.
[15] P. M. Carrica, H. Fu, and F. Stern, "Computations of self-propulsion free to sink and trim and of motions in head waves of the KRISO Container Ship (KCS) model," *Appl. Ocean Res.*, 2011.
[16] A. Mofidi and P. M. Carrica, "Simulations of zigzag maneuvers for a container ship with direct moving rudder and propeller," *Comput. Fluids*, vol. 96, pp. 191–203, 2014.
[17] A. Elhanafi, "Prediction of regular wave loads on a fixed offshore oscillating water column-wave energy converter using CFD," *J. Ocean Eng. Sci.*, vol. 1, no. 4, pp. 268–283, 2016.
[18] K. Niklas, "Strength analysis of a large-size supporting structure for an offshore wind turbine," *Polish Marit. Res.*, vol. 24, no. s1, Jan. 2017.
[19] A. Elhanafi, G. Macfarlane, and D. Ning, "Hydrodynamic performance of single-chamber and dual-chamber offshore-stationary Oscillating Water Column devices using CFD," *Appl. Energy*, vol. 228, no. March, pp. 82–96, 2018.
[20] Ulstein Design AS, "A foreship arrangement for a vessel of the deplacement type," WO 2006/096066 A1, 2006.
[21] J. H. Ferziger and M. Peric, *Computational Methods for Fluid Dynamics*. Springer, 2002.
[22] Y. C. Kim, K. S. Kim, J. Kim, Y. Kim, I. R. Park, and Y. H. Jang, "Analysis of added resistance and seakeeping responses in head sea conditions for low-speed full ships using URANS approach," *Int. J. Nav. Archit. Ocean Eng.*, vol. 9, no. 6, pp. 641–654, 2017.
[23] T. Tezdogan, Y. K. Demirel, P. Kellett, M. Khorasanchi, A. Incecik, and O. Turan, "Full-scale unsteady RANS CFD simulations of ship behaviour and performance in head seas due to slow steaming," *Ocean Eng.*, vol. 97, pp. 186–206, 2015.
[24] Siemens PLM Software, "User Guide Star CCM+ v12.04," 2017.
[25] ITTC, "ITTC Quality System Manual Recommended Procedures and Guidelines Preparation , Conduct and Analysis of Speed / Power Trials 7.5-04-01-01.1," 2017.